Nanoscale

Accepted Manuscript

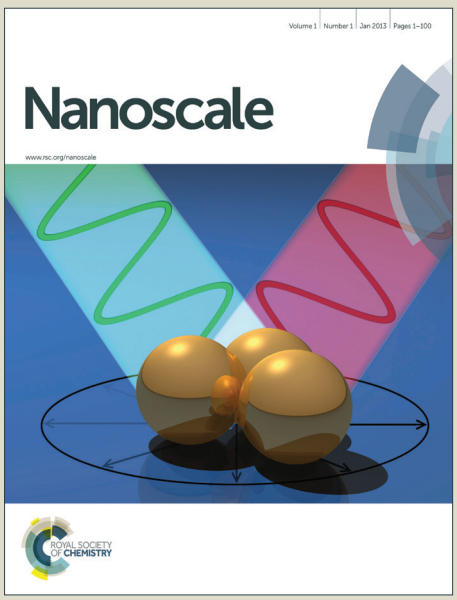

ROYAL SOCIETY OF CHEMISTRY

www.rsc.org/nanoscale

Nanoscale

RSCPublishing

ARTICLE

Giant Piezoresistivity in Aligned Carbon Nanotube Nanocomposite: Account for Nanotube Structural Distortion at Crossed Tunnel Junctions†

Cite this: DOI: 10.1039/x0xx00000x

S. Gong[a] and Z. H. Zhu*[a]

Received 00th January 2012,
Accepted 00th January 2012

DOI: 10.1039/x0xx00000x

www.rsc.org/

High piezoresistivity is critical for multifunctional carbon nanotube polymer composites with sensing capability. By developing a new percolation network model, this work reveals theoretically that a giant piezoresistivity in the composites can be potentially achieved by controlled nanotube alignment resulting from field based alignment techniques. The tube–tube and/or tube–matrix interaction in conjunction with the aligned carbon nanotube networks are fully considered in the newly proposed model. The structural distortion of nanotubes is determined self-consistently by minimizing the pseudo-potential energy at crossed-tube junctions based on the Lennard-Jones potential and simulation of coarse grain molecular dynamics. The tunneling transport through crossed-tube junctions is calculated by the Landauer-Büttiker formula with empirical fitting by first-principle calculation. The simulation results also reveal that the piezoresistivity can be further improved by using low carbon nanotube loadings near percolation threshold, carbon nanotubes with small aspect ratio, high intrinsic conductivity and, polymers with small Poisson's ratio. This giant piezoresistive effect offers a tremendously promising future, which needs further thorough exploration.

Introduction

Carbon nanotubes (CNTs) enhanced polymer composites exhibit great potential for a variety of applications, such as microelectronic devices, condition monitoring through strain sensing, and chemical and biological sensors.[1-5] Compared with the conventional piezoresistive sensing materials, such as metals, alloys, and inorganic semiconductor materials, sensors made of multifunctional CNT/polymer composites are lightweight, compact, mechanically durable and easily conformable for desired shapes and applications. For instance, they can be directly embedded in structural composites to provide real-time internal strain sensing for structural health monitoring.[4] However, these CNT-based sensing composites are still far from real applications. The requirement for high sensitivity is one of the major challenges in this regard. Aligning CNTs inside the host polymer matrix was considered an effective strategy to improve physical properties in the CNT alignment direction. Enhancement effects have been found in mechanical and electrical properties of these composites. For example, the alignment of CNTs under a 25 *Tesla* magnetic field in MWCNT(multi-walled CNT)/epoxy composites leads to a 35% increase in electric conductivity compared to those without alignment.[6] Andrews et al. fabricated drawn isotropic petroleum pitch/SWCNT(Single-walled CNT) composite fibers with 5 wt.% CNT loadings.[7] The tensile strength and modulus of the fibers were increased by 90 and 150%, respectively, due to the CNT alignment. Up to date, the potentiality of piezoresistive property enhanced by CNT alignment in the CNT/polymer composites is still not thoroughly explored.

The piezoresistive property of CNT/polymer composites is represented by the relative change of their electrical conductivity under strain. The electrical conductivity of CNT/polymer composites depends heavily on the morphology of random CNT networks and the properties of CNTs and crossed-tube junctions that form the networks. Currently, theoretical studies of electrical properties generally focus on the ballistic transport of CNTs with the perfect honeycomb arrangement of carbon atoms.[8-14] Recent investigations have shown that the structural distortion of CNTs could substantially affect local electrical structure and act as a strong scatter to reduce the intratube conductance. For example, Tombler et al. observed large and reversible variations in electrical conductivity of metallic CNTs by mechanically deforming the tubes with an atomic force microscope.[15] The study showed that the configuration of local bonding changed from sp^2 to nearly sp^3 in the highly distorted local region. Nardelli and Bernholc noted theoretically that the bending deformation of CNTs could alter their band gap, depending on their chirality.[16] Rochefort et al. found that the increased bending deformation of nanotubes could enhance the states of local density of σ and π electrons as well as σ–π mixing and rehybridization, leading to a charge polarization of the C–C bonds in the distorted region.[17] Scattering of conduction electrons in the distorted regions may result in the electron localization. It was found by Minot et al. that the bond strain could open a band gap in a metallic tube and modify the band gap in a semiconducting tube.[18] On the other hand, intertube distance reduction at relaxed CNT junctions resulting in a large overlap of wave functions, which will favor intertube tunneling and increase the contact conductance. It is revealed experimentally by Fuhrer et al. that the transmission probability between two contacting metallic carbon nanotubes increased by 200 times from 2×10^{-4} to 0.04 due to the radial indentation of CNT walls induced by a contact

force being estimated only 5 nN.[19, 20]

The structural distortions could be the result from the interaction of tube–tube or tube–matrix. It is well known that CNTs are extremely rigid in the axial direction but are very likely to distort perpendicular to the axis.[21-23] The Young's moduli of both MWCNTs and SWCNTs in radial direction are in the same order of polymer's (several GPa). CNTs with localized kinks and bends, as well as radial indentations, have been observed in polymer matrices.[24] However, the effects of the local structural distortions of CNTs on electrical properties of CNT/polymer composites, especially with CNT alignment, are still not fully investigated. To the best of our knowledge, there is little theoretical study to systematically investigate the piezoresistivity in the aligned CNT/polymer composites. In view of earlier findings that the structural distortion can influence the conductance in CNTs and tunneling effect at CNT-CNT junctions, the combination of the unique CNT strain sensing characteristics and aligned CNT network may lead to novel and high performance electromechanical multifunctional devices.

In this work, a new percolation network model that considers the structural distortion of CNTs and tube–tube and/or tube–matrix interaction due to the van der Waals and dipole–dipole interactions in the aligned CNT networks was developed. The structural distortion of CNTs is determined self-consistently by minimizing the pseudo-potential energy at the CNT crossed junctions based on the Lennard-Jones potential and simulation of coarse-grained molecular dynamics.[25] The tunneling transport through crossed-tube junctions is calculated by the Landauer-Büttiker formula with Wentzel–Kramers–Brillouin approximation, while the work function of distorted CNTs is obtained by empirical fitting of first-principle calculation.[26] With these improvements, theoretical predictions of electrical properties in CNT/polymer composites agree with experimental data much better than the existing percolation network theory, which usually overestimates the electrical conductivity and underestimates piezoresistivity. The theoretical analysis of the strain-induced electrical conductivity indicates that a giant piezoresistivity, relative to the conventional strain sensors, can be achieved by properly controlling the orientation alignment of CNTs in the percolation networks in polymer matrix. While the CNTs are properly aligned in certain directions, simulation results show that the variations of intertube distance and structural distortion of CNTs by external strains could induce further changes in both intertube tunneling conductance and intratube intrinsic conductance. This giant piezoresistivity of aligned CNT/polymer composites could be potentially useful in applications of high-sensitive electromechanical systems and in the design of high performance electronic devices.

Modelling formulation

New CNT percolation networks

In this study, the electrical conductivity of CNT/polymer composites is modeled based on the percolation theory, which has been widely used in simulations of CNT network systems.[10-14] Consider a 3-dimensional (3D) CNT percolation network model containing uniformly distributed and aligned CNTs in the polymer matrix as shown in Figure 1a and 1b, respectively. The CNT percolation network theory assumes the resistivity of the percolating CNT networks in the composite can be represented by the resistivity of an effective resistor network, where the CNTs that do not participate in conducting current flow are eliminated by the Dulmage–Mendelsohn decomposition.[27] Then, the conductivity of the resistor network is evaluated by the Kirchhoff's circuit law when a critical tube concentration, the percolation threshold, is reached to form conductive pathways in the polymer matrix.[28-30]

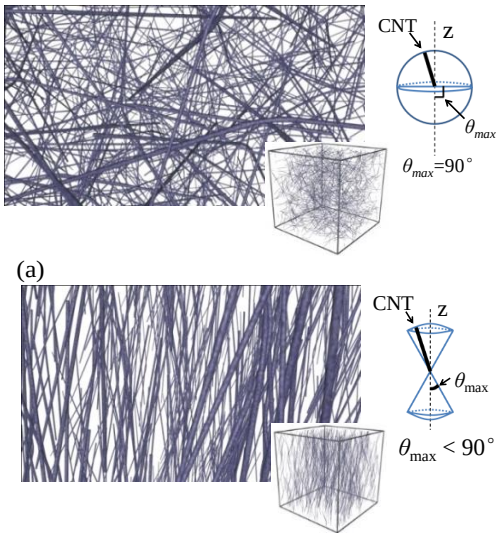

Figure 1. Schematics of (a) uniformly distributed and (b) typical aligned CNT networks with θ_{max} = 35°.

The percolation network model assumes that CNTs are randomly located in the networks while the lengths of nanotubes obey a Weibull distribution.[27] Each CNT in the model is assumed straight initially and described by a line segment with the starting (x_i^0, y_i^0, z_i^0) and ending (x_i^1, y_i^1, z_i^1) points, such that,

$$\begin{Bmatrix} x_i^1 \\ y_i^1 \\ z_i^1 \end{Bmatrix} = \begin{Bmatrix} x_i^0 \\ y_i^0 \\ z_i^0 \end{Bmatrix} + l_i \begin{Bmatrix} \sin\theta_i \cos\beta_i \\ \sin\theta_i \sin\beta_i \\ \cos\theta_i \end{Bmatrix} \quad (1)$$

where i refers to the i-th CNT, l_i is the CNT length that obeys the Weibull distribution $l_i = F^{-1}(rand)$, $F(x) = 1 - \exp\left[-(x/a)^b\right]$ for $x \geqslant 0$, (a, b) are the parameters of Weibull distribution, and (β_i, θ_i) are the azimuthal and polar angles of CNT in space, respectively.

The CNT alignment is described by varying the azimuthal and polar angles within their respective ranges [0, 2π], [cosθ_{max}, 1] and [−1, cos(π−θ_{max})], such that,

$$\beta_i = 2\pi \times rand,$$

$$\theta_i = \begin{cases} \pi - 2\theta_{max} + \dfrac{2\theta_{max}}{\pi}\cos^{-1}(2\times rand - 1) & 0 \le rand < 0.5 \\ \dfrac{2\theta_{max}}{\pi}\cos^{-1}(2\times rand - 1) & 0.5 \le rand \le 1 \end{cases} \quad (2)$$

where '*rand*' denotes uniformly distributed random numbers in the interval [0, 1], and θ_{max} is the maximum CNT alignment angle in the range [0, π/2], which is used to evaluate the extent of alignment.

The alignment of CNTs in a polymer matrix could be affected by either (i) ex-situ alignment methods,[31] such as growing homogeneous and well-aligned arrays of CNTs using chemical vapor deposition method or (ii) mechanical force, electrical and/or magnetic field based alignment techniques.[32-34] The former produces uniformly aligned CNTs on a selected

substrate, which can be simply modeled as parallel conductive paths.[35] The latter results in the orientation of each CNT is randomly distributed within a range limited by the maximum alignment angle (θ_{max}) ranging from 0° to 90°, where the 0° represents the CNTs are fully aligned or parallel while the 90° means the CNTs are completely non-aligned. The maximum alignment angle can be tuned over a broad range by properly controlling the applied field strength, frequency, and duration.[36] Our analysis in this paper is conducted in accordance with the controlled CNT alignment structure achieved by the field based alignment techniques.

Electron transport of CNTs and crossed-tube junctions

The distance between each CNT pair is evaluated to check if the crossed-tube junction is formed. In our model, all the tubes are assumed straight initially and the nanotube structural distortion at crossed junctions are considered. The geometric configuration at junction is determined by minimizing a constrained total energy. In that process, the position of the atoms near the junction is fully relaxed while the center-to-center tube distance (d) is fixed, see Figure 2a. If d is smaller than the CNT diameter (D) plus the van der Waals distance (d_{vdw}), the tube wall will bend (Figure 2d and 2e) to avoid either penetrating each other (Figure 2b) or underestimating tube-tube interaction (Figure 2a). Note that only the bending of CNT at the crossed-tube junction is considered in the current work. The rest of CNT away from the junction is assumed straight. The total pseudo potential energy (E) of the junction can be expressed by $E = 2E_b + E_{LJ}$, where E_b is the energy associated with the bending of CNT walls and E_{LJ} is the Lenard–Jones (L-J) potential associated with the van der Waals interaction between CNTs, respectively. The local structural distortions of CNTs and the separation gap between two distorted CNT walls are determined self-consistently by minimizing the total energy (ESI†). Results show that the separation gap in an effective contact region of two CNTs reaches an extreme at nearly 0.26 nm, which is roughly the same as the one reported in Ref. 20. Any further decrease in the distance d will bend the CNT walls over a larger area rather than decrease the gap between CNT walls.

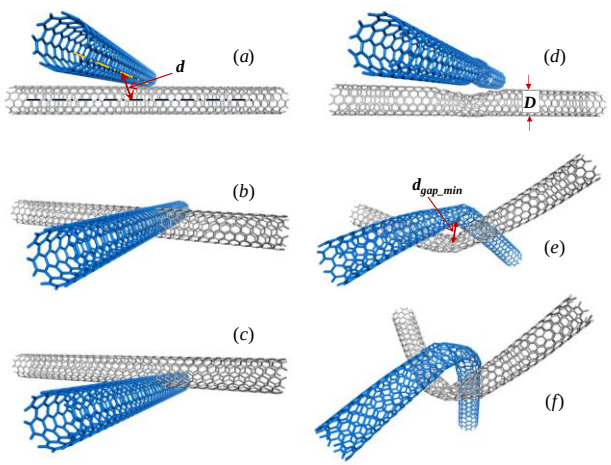

Figure 2. Schematics of rigid CNT junctions (*a*, *b*) and corresponding relaxed CNT junctions (*d*, *e*). Under external strains, the wall deformable CNTs would further bend at the junction (*f*) instead of penetrating each other (*c*).

The effect of structural distortion on the intrinsic resistance R_{int} of a uniform CNT with diffusive scattering is evaluated as:

$$R_{int} = \int_0^l \frac{4}{\pi (D')^2 \sigma_{cnt} \exp[-\eta(1 - D'/D)]}\, dl \qquad (3)$$

where l is the length of the CNT segment, σ_{cnt} is the intrinsic electrical conductivity with perfect honeycomb carbon arrangements, D' is the nominal diameter of bent CNT and η is the change rate of conductivity which can be determined experimentally.[37] For instance, η = 32 for (12, 0) CNTs. The contact region at crossed-tube junctions is at the nanoscale, which is less than the momentum relaxation distance and the Fermi wavelength. As such, the tunneling current can be described by the Landauer-Büttiker formula with the effect of spin degeneracy included:[27]

$$I = \frac{2e}{h}\int_0^\infty \mathrm{T}(E) M(E) \left[\frac{1}{e^{\frac{E-\mu-eV}{k_B T}} + 1} - \frac{1}{e^{\frac{E-\mu}{k_B T}} + 1} \right] dE \qquad (4)$$

where $M(E)$ denotes the total conduction channel number and $\mathrm{T}(E)$ the electron transmission probability. Both of them are functions of electron energy level E. Furthermore, the quantities μ and T represent the chemical potential and the temperature of CNTs. The rest of the constants are the electron charge e, Planck's constant h and Boltzmann constant k_B. Under a low bias voltage V, the above equation can be approximated asymptotically by using the first-order Taylor expansion. Assume that the simulations are carried out at 300 K and the channel number M is an integer that is independent on the electron energy level, the tunneling resistance R_t can be evaluated from the averaged tunneling model, such as:

$$R_t \approx \frac{h}{2e^2} \cdot \frac{1}{M\mathrm{T}} \qquad (5)$$

It is known that each conduction channel contributes to the total conductance if the tunneling distance is smaller than the electron mean free path. For a metallic SWCNT, there are two bands crossing the Fermi level. Thus, two channels are expected for a metallic SWCNT. For a MWCNT, experimental work reveals that the channel numbers (about 460) is much larger than SWCNT due to the participation of multiple walls in the electrical transport and the large diameter of nanotubes.[38] The transmission probability is assessed using the Schrödinger equation with a rectangular potential barrier assumption or from the approximation of Wentzel–Kramers–Brillouin, such as:[28]

$$\mathrm{T} = \begin{cases} \exp\left(\dfrac{-d_{gap\_\min}}{h/\sqrt{8m_e W'_{cnt\_\min}}} \right) & 0 < d \le (2D'_{\min} - D) + d_{gap\_\min} \\ \exp\left(\dfrac{-d_{gap}}{h/\sqrt{8m_e W'_{cnt}}} \right) & (2D'_{\min} - D) + d_{gap\_\min} < d \le D + d \\ \exp\left(\dfrac{-(d - D)}{h/\sqrt{8m_e W_{cnt}}} \right) & D + d_{vdw} < d \le D + 2d_{vdw} \\ \exp\left(\dfrac{-(d - D - 2d_{vdw})}{h/\sqrt{8m_e (W_{cnt} - W_{polymer})}} + \dfrac{-2d_{vdw}}{h/\sqrt{8m_e W_{cnt}}} \right) & D + 2d_{vdw} < d \le d_{cutoff} \end{cases} \qquad (6)$$

where m_e is the electron mass, d_{gap} is the separation gap between two distorted CNT walls, W_{cnt} and $W_{polymer}$ are the work functions of CNTs and polymer matrix, W'_{cnt} is the work function of distorted CNTs and is approximated by empirical fitting of first-principle calculation, d_{cutoff} is the maximum effective distance of tunneling effect, respectively.[26] d_{gap_min}, D'_{min} and W'_{cnt_min} are corresponded to the critical states from total energy minimization where CNTs start to bend over a larger area instead of further reduce the separation gap.

Piezoresistive behavior under external strain

The piezoresistive behavior of the CNT/polymer composites is characterized by the strain gauge factor (K). It is calculated by comparing the electrical resistance changes with respect to the applied strain ($\Delta\varepsilon$), such that,

$$K = \frac{\Delta R / R_0}{\Delta\varepsilon} \quad (7)$$

where R_0 is the electrical resistance before strain and ΔR is the external strain induced variation of electrical resistance. To evaluate the new state of the CNT networks deformed by a small uniaxial strain ($\Delta\varepsilon$ < 0.01), the following commonly accepted assumptions are adopted.[11, 14, 39] First, the CNTs are assumed not stretchable or compressible in the axial direction since the axial Young's modulus of CNTs is much greater than that of polymer matrix. The interfacial shear stress between CNT and polymer has been neglected. Second, the aggregation of CNTs is neglected and CNTs are assumed to change their orientations and positions only after the straining process by the 3D fiber reorientation model based on an affine transformation.[40] The effect of local shear strain in the straining process is neglected. Third, the Poisson's ratio of aligned CNT/polymer composites is assumed anisotropic and modeled by a simple micromechanics model.[41]

If CNTs are randomly dispersed in the matrix ($\theta_{\max} = \pi/2$), the Poisson's ratio of the CNT/polymer composites is approximated by the Poisson's ratio of polymer for simplification. If CNTs are well aligned in the direction z with $\theta_{\max} = 0$, the Poisson's ratios of CNT/polymer composites are:

$$\begin{aligned} &v_{zx}^0 = v_{zy}^0 = v_{cnt}V_{cnt} + v_{polymer}(1 - V_{cnt}) \\ &v_{xz}^0 = v_{yz}^0 = v_{zx}^0 E_x / E_z \\ &v_{xy}^0 = v_{yx}^0 = 0.3 \end{aligned} \quad (8)$$

with

$$\begin{aligned} &E_z \approx E_{cnt}V_{cnt} \\ &E_x = E_y \approx E_{polymer}(1 - V_{cnt})^{-1} \end{aligned} \quad (9)$$

where V_{cnt} is the volume fraction of CNT in CNT/polymer composites. E_{cnt} and v_{cnt} is the axial Young's modulus and Poisson's ratio of CNT, $E_{polymer}$ and $v_{polymer}$ is the Young's modulus and Poisson's ratio of polymer matrix, respectively.

While $\theta_{\max}$ varies in the range (0, π/2), the Poisson's ratios of CNT/polymer composites are calculated based on the angle, such as:

$$\begin{aligned} &v_{zx} = v_{zy} = v_{zx}^0 + \frac{2}{\pi}\left(v_{polymer} - v_{zx}^0\right)\theta_{\max} \\ &v_{xz} = v_{yz} = v_{xz}^0 + \frac{2}{\pi}\left(v_{polymer} - v_{xz}^0\right)\theta_{\max} \\ &v_{xy} = v_{yx} = 0.3 \end{aligned} \quad (10)$$

Accordingly, the new position of CNT midpoint subject to an incremental strain $\Delta\varepsilon$ can be derived as:

$$\begin{aligned} &(x', y', z') = (x - xv_{zx}\Delta\varepsilon, y - yv_{zy}\Delta\varepsilon, z + z\Delta\varepsilon) \text{ or} \\ &(x', y', z') = (x + x\Delta\varepsilon, y - yv_{xy}\Delta\varepsilon, z - zv_{xz}\Delta\varepsilon) \text{ or} \\ &(x', y', z') = (x - xv_{yx}\Delta\varepsilon, y + y\Delta\varepsilon, z - zv_{yz}\Delta\varepsilon) \end{aligned} \quad (11)$$

The movement of CNT junctions can be evaluated by calculating new orientations and positions of CNTs after the strain is applied. Under the local strain, CNTs could further bend at junctions (Figure 2f) rather than penetrate each other (Figure 2c) when they are pushed together. This may occur under both tensile and compressive strains due to the effect of the Poisson's ratio.

Results and discussion

Validation of new CNT percolation network model

The validation of the new CNT percolation network model was conducted by Monte Carlo simulations. The parameters of CNTs and polymer used in simulation are given in Table 1. Other parameters are shown in the corresponding figures, such as the conduction channel numbers, length, and diameter of CNTs. Because of the unique one-dimensional structure of CNTs, a high anisotropy is expected for CNT/polymer composites when CNTs are aligned in certain directions. Thus, the electrical properties are measured in two typical directions: (i) parallel with "||" and (ii) perpendicular to "⊥" the CNT alignment direction. In addition, the maximum alignment angle θ_{max} is expressed in term of degrees for easy understanding.

Table 1. Physical parameters of CNT/polymer composites.

Items	Values	Refs.
Electrical conductivity of CNT, σ_{cnt}	10^3~10^6 S/m	39
Van der Waals distance, d_{vdw}	0.34 nm	42
Cutoff distance, d_{cutoff}	1.4 nm	27
Work function of CNT, W_{cnt}	4.7 eV	28
Work function of polymer, $W_{polymer}$	3.75~4.5 eV	43
Poisson's ratio of CNT, v_{cnt}	0.236	9
Poisson's ratio of polymer matrix, $v_{polymer}$	0.1~0.5	28
Axial Young's modulus of CNT, E_{cnt}	1 TPa	39
Young's modulus of polymer matrix, $E_{polymer}$	1~10 GPa	9

The simulated electrical conductivities of SWCNT/polymer composites are shown in Figure 3 with respect to CNT alignment. The insert in Figure 3 shows the electrical conductivities of randomly dispersed CNT samples (θ_{max} = 90°) with different CNT loadings. It is clear that the newly developed percolation network model is in good agreement with the experimental data.[44] It is worth to note that CNTs were considered either as ''soft-core" or "hard-core" in the existing percolation network models.[10-14] The former led to a physically incorrect CNT overlap or penetration at CNT junctions,[39] while the latter assumed CNTs as rigid and non-deformable tubes.[45] All of them ignored the effect of CNT structural distortion and thus overestimated the electrical conductivity by orders of magnitude.[19, 20] Our study finds that, for the relaxed metal SWCNT junctions, the total conductance near a structurally distorted junction is approximately two orders of magnitude lower than that of a rigid junction, showing the importance of the structural distortion at junctions.

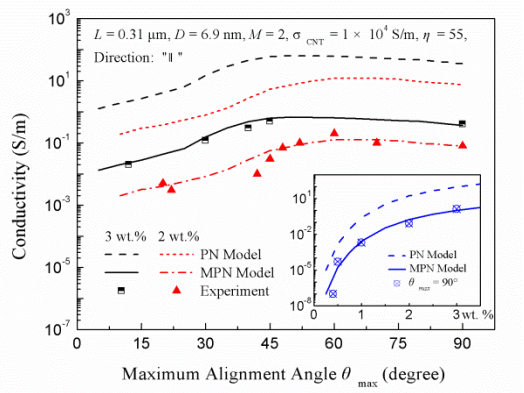

Figure 3. Comparison of simulation results and experimental data of electrical conductivities in SWCNT/polymer composites.[44] PN – existing percolation network model; MPN – newly developed percolation network model.

Next, the simulation results of strain gauge factors of MWCNT/polymer composites are compared with experimental data with different CNT loadings subject to both tensile and compressive strains (up to ±0.006).[46] As shown in Figure 4, the strain gauge factors of the MWCNT/polymer composites exhibit different characteristics in tension than compression. Very high piezoresistive sensitivity can be achieved when subject to tensile strain; especially the CNT loading is near the percolating threshold. As the CNT loading increases more than 10 wt.%, the gauge factors decrease quickly to 2, a value of conventional strain gauges, as the CNT/polymer composites become very conductive. Existing percolation model cannot predict these characteristics correctly, because it considered only two piezoresistive mechanisms of composites under external strain.[10-14] One of the mechanisms is the length change of CNT segments that participate in conducting the current flow in reorientation process. The length change is caused by the movement of CNT junctions. The other is the intertube distance change at crossed CNT junction. With the rigid CNT assumption, there will be no resistance change if the shortest intertube distance is less than d_{vdw}. According to our new percolation network model, the contact resistance could be further reduced as the intertube distance is decreased from d_{vdw} (about 0.34nm) to d_{gap_min} (near 0.28nm) at relaxed CNT junctions. Furthermore, the variation of CNT structural distortion due to strain cannot be ignored. Both the transmission probability for intertube tunneling and the electrical transport on intratube are highly related to the CNT structural deformation. With all of these mechanisms considered, the simulation results of model agree with the experimental data much better than existing models.

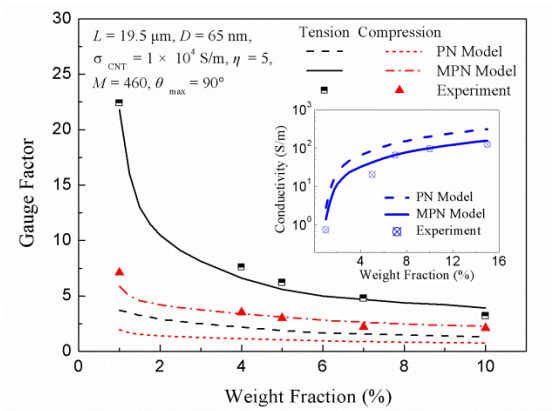

Figure 4. Comparisons of predicted and experimental electrical conductivity and piezoresistivity of MWCNT/polymer composites.[46] PN – existing percolation network model; MPN – newly developed percolation network model.

Giant piezoresistive effect in aligned CNT/polymer composites

The giant piezoresistive effect due to CNT alignment is shown numerically in Figure 5 where the electrical conductivity of MWCNT/polymer composites is plotted versus CNT alignment. The parameters used for the MWCNT/polymer composites are adopted for all simulations in the following sections. Figure 5a shows that higher conductivity has been achieved in the direction parallel with the CNT alignment than the direction perpendicular to the CNT alignment. This is likely because the CNTs themselves provide more conductive paths in the direction parallel with alignment than perpendicular to the alignment due to the high aspect ratio of CNTs. Furthermore, the polymer matrix between CNTs separates them in the perpendicular direction also leads to the lower conductivity in this direction. Up to date, there is only limited experimental data available in this area. It should be noted that the experimental data were measured from the samples either with uniformly aligned CNTs grown on a selected substrate or with obviously aligned CNT aggregation. The former had different CNT network structure than our model and the later led to a significant low conductivity than the theoretical predictions by existing models due to the CNT aggregation. Compared with the limited available experimental data at θ_{max} = 10°, the present simulation results show a good agreement with the experimental data, which indicates the validation and robustness of the newly proposed percolation network model.[47] Furthermore, the average conductive pathway densities of unit cross section at different directions are shown in Figure 5b. It shows the same characteristics as the electrical conductivity in both directions, which indicates that the conductive pathway density is a key parameter for electrical properties of aligned CNT composites. When the CNTs are highly aligned, e.g., θ_{max} < 30°, the opportunity to form conductive paths by crossed-tube junctions is reduced significantly, leading to a sparse conductive network in both two directions. The results indicate that the CNT alignment is an effective way to tune the electrical properties of CNT/polymer composites.

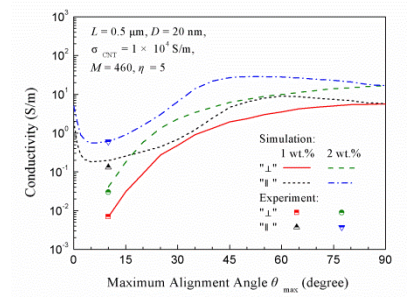

(a)

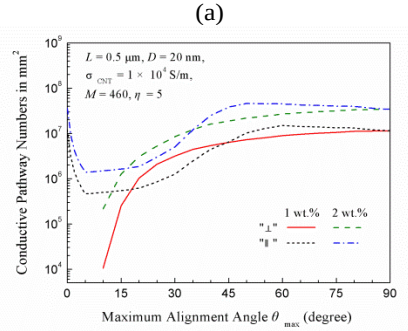

(b)

Figure 5. Electrical conductivities vs CNT alignment angle: (a) resistance change ratios and (b) corresponding conductive pathway density.

Next, the anisotropic characteristic in the piezoresistive behavior of aligned CNT/polymer composites is investigated. Figure 6 shows the piezoresistivity of CNT/polymer composites with 1 wt.% CNT loading versus the maximum CNT alignment angle. The resistance change ratios are nonlinear with respect to the external strain in the direction parallel with the alignment, especially with small values of θ_{max}. While in the perpendicular direction, it shows an approximately linear relationship with respect to the applied strain. More interestingly, the aligned CNT/polymer composites exhibit giant piezoresistive effect

with small values of θ_{max}, which have not been revealed by experiments yet. For instance, it is noted that the resistance change ratio reaches the maximum and minimum at θ_{max} = 20° and θ_{max} = 90° respectively for a given strain in the direction parallel to the CNT alignment, and the maximum and minimum at θ_{max} = 10° and θ_{max} = 60° respectively in the direction perpendicular to the CNT alignment.

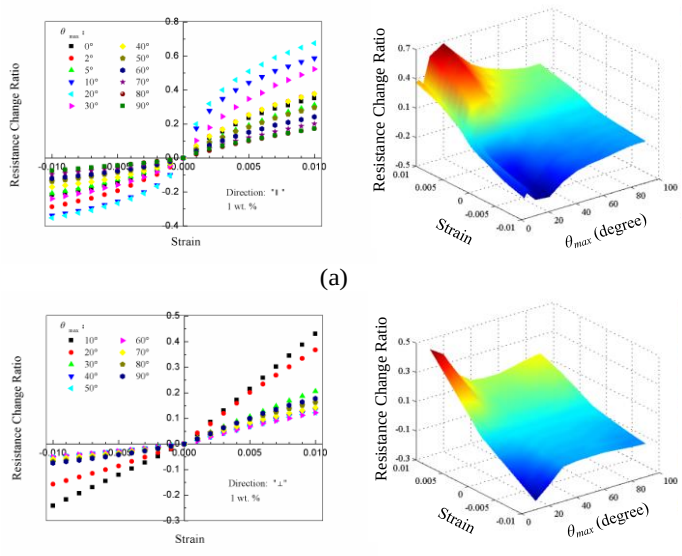

Figure 6. The directional effect of CNT alignment on the resistance change ratio: (a) parallel and (b) perpendicular to the alignment of the CNTs.

Lastly, the relationship of strain gauge factor vs CNT alignment angle is shown in Figure 7, whereas the relative change ratios of conductive pathway density in both directions are shown as an insert in the figure. As shown in the insert, when the CNTs are highly aligned, e.g., θ_{max} < 30°, the relative change ratios of conductive pathway density in both directions increase significantly. This leads to a significant increase in the strain gauge factor in both directions with the same trends. For instance, the gauge factors of the composites with θ_{max} = 20° are enhanced by 390% and 470% in the parallel direction as well as 210% and 200% in the perpendicular direction under the tensile and compressive strains, respectively, due to the alignment of CNTs. This indicates that the giant piezoresistivity can be achieved by the controlled CNT alignment with small values of θ_{max} in CNT/polymer composites.

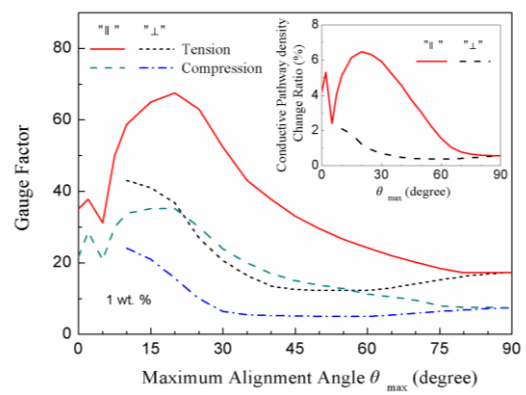

Figure 7. Strain gauge factor and change ratio of conductive pathway density vs. CNT alignment angle.

Mechanism of giant piezoresistive effect

After revealing the giant piezoresistive effect, we will attempt to understand the mechanisms behind it by decomposing the total resistance (R_{tot}) of the CNT/polymer composites into different components. As described before, the truly ballistic transport in CNTs may require straight tubes. Any structural distortion of CNTs could modify the nanotube's electrical structure, which is expected to scatter the conduction electrons at the distorted regions resulting carrier localization, especially at low temperatures. Thus, there are three resistance components in CNT networks, namely, the intratube resistance generated by ballistic transport (R_b), the intratube resistance results from CNT structural distortion (R_d) and the intertube tunneling resistance (R_t) at crossed CNT junctions. Figure 8 shows the variations of the total resistance as well as its components versus the CNT alignment.

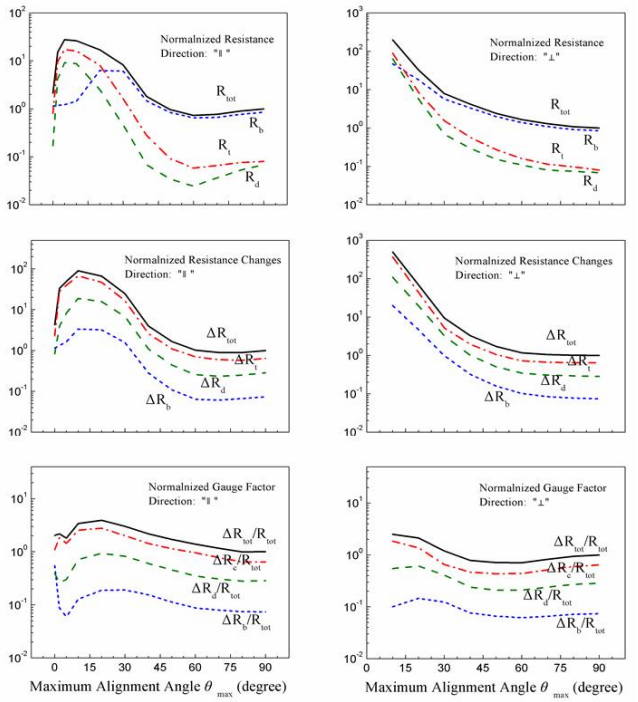

Figure 8. Resistance components in the total resistance, resistance change and gauge factor of 1 wt. % aligned MWCNT/polymer composites, normalized by the corresponding data at θ_{max} = 90°.

Under applied external strains, the CNT network morphology is changed due to the CNT reorientation process. The variation of intratube resistance generated by the ballistic transport ΔR_b results from the length change of perfectly straight CNT segments that participate in conducting the current flow. The variation of the intertube tunneling resistance ΔR_t depends nontrivially on the intertube distance. For example, a larger gap between nanotubes results in a smaller overlap of wave functions and consequently a larger tunneling resistance. Indeed, the junction resistance is a result of interaction between intratube and intertube transmissions. Both of them depend on local distorted region at the junction, which is also affected by the local strain. As shown in Figure 8, the variations of intertube tunneling resistance (ΔR_t) and intratube resistance

induced by CNT structural distortion (ΔR_d) are the two primary mechanisms for the piezoresistivity of aligned CNT/polymer composites. With the small values of θ_{max} (i.e. 10° < θ_{max} < 30°), the composite exhibits an obvious giant piezoresistive effect, as expected from the relatively high proportion of R_t and R_d in R_{tot}.

Further improvement of giant piezoresistive effect

In this section, the effects of the same important parameters, such as the CNT loadings, CNT morphology, electrical properties of CNTs, work function and Poisson's ratio of polymer on the piezoresistivity are studied in the presence of CNT alignment to explore the ways for further improvement of the giant piezoresistive effect in the aligned CNT/polymer composites.

At first, the effects of CNT loadings on the piezoresistive behavior of the aligned CNT/polymer composites are shown in Figure 9. The percolation threshold of the CNT/polymer composite in this case is found as low as 0.25 wt. %. Continuous increase of gauge factor appears in all aligned CNT/polymer composites when the CNT loading decreases form 5 wt.% to 0.25 wt.%. As the CNT loading increased beyond 2 wt.%, the variation of gauge factor versus CNT alignment angle becomes monotonic and the piezoresistivity peaks at low θ_{max} (θ_{max} = 10°) in both directions. A very high gauge factor (greater than 100) can be achieved as the CNT loading near the percolating threshold. For the purpose of maximizing the piezoresistive sensitivity in the composites, the CNT alignment structure corresponding to the peak gauge factor should be chosen for each CNT loading.

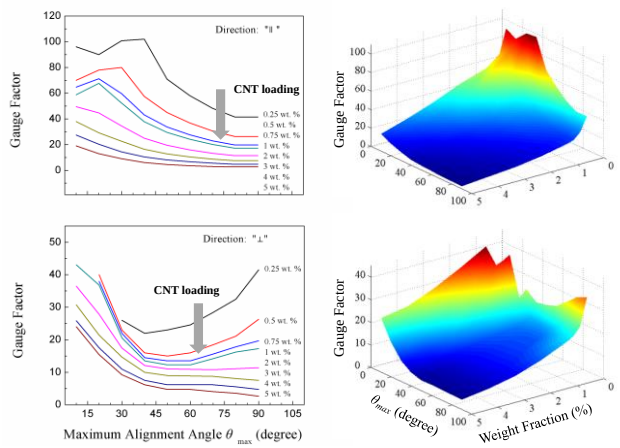

Figure 9. Influences of CNT loadings on the gauge factor of the aligned CNT/polymer composites in the parallel and perpendicular directions.

Next, simulations are conducted for the CNT lengths ranging from 0.5 to 2.5 μm for a fixed CNT diameter of 20 nm, while the remaining parameters are kept the same. The simulation results reveal a steady decrease of gauge factors as the CNT aspect ratio increases, as shown in Figure 10. It is generally agreed that the composites with larger CNT aspect ratio have higher electrical conductivity and lower piezoresistive sensitivity because there is a higher probability to form CNT junctions in polymer matrix. On the other hand, CNTs can either be conducting or semiconducting depended on tubes' chirality. The typical range of CNT intrinsic conductivity reported by experiments is from 10^3 to 10^6 S/m.[27] Our simulation results also indicate that, while CNT intrinsic conductivity varies within the above range, the gauge factor increases significantly in proportion with the CNT intrinsic conductivity.

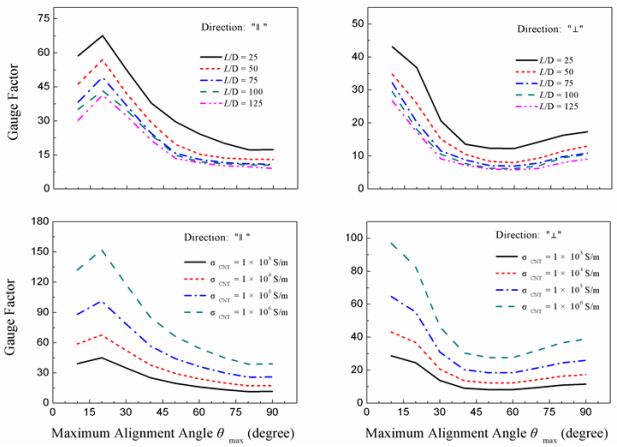

Figure 10. Influences of morphology and electrical conductivity of CNTs on the gauge factor of the aligned CNT/polymer composites.

Finally, the influences of polymer matrix properties on the piezoresistive property are shown in Figure 11. The polymers' work functions vary from 3.75 to 4.5 eV, with the typical values for nylon 66, polystyrene, polycarbonate, and polyimide are 3.95 eV, 4.22 eV, 4.26 eV, and 4.36 eV, respectively.[28] Simulation results show that the polymer's work functions have limited effects on the piezoresistive property of aligned CNT/polymer composites in both directions. The major and minor Poisson's ratios of aligned CNT/polymer composites are affected by the Poisson's ratio of polymer matrix. The gauge factors increase monotonically as the Poisson's ratio of polymer $\nu_{polymer}$ increased from 0.1 to 0.5 in the perpendicular direction. In the parallel direction, the Poisson's ratio of polymer $\nu_{polymer}$ has an opposite effect on the gauge factors of highly aligned CNT/polymer composites (small θ_{max}) and near randomly dispersed CNT/polymer composites (θ_{max} > 75°). It indicates that the smaller $\nu_{polymer}$ helps to improve the piezoresistivity of the highly aligned CNT/polymer composites.

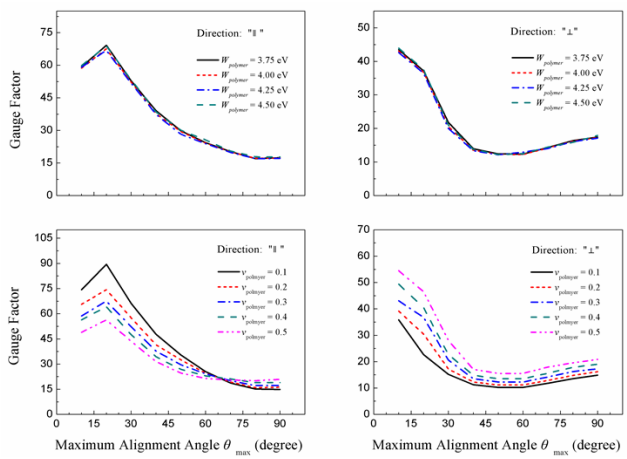

Figure 11. Influences of work function and Poisson's ratio of polymer matrix on the gauge factor of the aligned CNT/polymer composites.

According to the above calculations, the giant piezoresistivity in CNT/polymer composites could be achieved by choosing lower CNT loading near percolation threshold, smaller aspect ratio and higher intrinsic conductivity of CNTs, and smaller alignment angle of CNTs. In addition, the anisotropy of piezoresistivity in CNT/polymer composites can be tuned by changing the Poisson's ratio of polymer matrix. The giant piezoresistive effect revealed in the aligned CNT/polymer composites makes them ideal candidates for future multifunctional materials that combine adaptive and sensing capabilities.

Conclusions

By developing a new CNT percolation network model, the paper demonstrated theoretically that a giant piezoresistivity in the CNT/polymer composites could be achieved by controlled CNT alignment resulting from field based alignment techniques. By considering the effect of structural distortion of CNTs in the intratube and intertube conductance in conjunction with the controlled CNT alignment in the newly proposed percolation network model, the new model predicts a lower electrical conductivity and higher piezoresistivity of CNT/polymer composites, which agrees better with experimental data than existing CNT percolation models. The analysis shows that the external strain induced changes of intertube tunneling resistance and intratube resistance related to the CNT structural distortion are two primary mechanisms for the piezoresistivity of CNT/polymer composites. The piezoresistivity of CNT/polymer composites is found to peak at a lower maximum alignment angle ($\theta_{max} < 30^0$) by four-to-five fold than that of CNT/polymer composites without CNT alignment. It is also found that the giant piezoresistivity can be further improved (gauge factor greater than 100) by choosing (i) CNTs with smaller aspect ratio and higher intrinsic conductivity, (ii) lower CNT loadings near percolation threshold, and (iii) polymers with smaller Poisson's ratios. Due to its high-sensitivity to applied strains, the aligned CNT/polymer composites have great potential for applications in strain sensors, transducers, and other multifunctional systems.

Acknowledgements

This work is supported by the Natural Sciences and Engineering Research Council of Canada (NSERC) and Canadian Space Agency.

Notes and references

[a] Department of Earth and Space Science and Engineering, York University. 4700 Keele Street, Toronto, ON, M3J 1P3, Canada.
* Email: gzhu@yorku.ca. Tel.: +1 416 736 2100 ext. 77729, Fax: +1 416 736 5817.
† Electronic Supplementary Information (ESI) available. See DOI: 10.1039/b000000x/

1 X. Wang, N. Behabtu, C. C. Young, D. E. Tsentalovich, M. Pasquali, J. Kono, *Adv. Funct. Mater.*, 2014, **24**, 3241.
2 B. Sun, Y. Z. Long, S. L. Liu, Y. Y. Huang, J. Ma, H. D. Zhang, G. Z. Shen and S. Xu, *Nanoscale*, 2013, **5**, 7041.
3 L. Jiang, S. Gu, Y. Ding, F. Jiang and Z. Zhang, *Nanoscale*, 2014, **6**, 207.
4 W. Obitayo, T. Liu, *J. Sens*., 2012, **2012**, 15.
5 C. Gao, Z. Guo, J. H. Liu and X. J. Huang, *Nanoscale*, 2012, **4**, 1948.
6 E. S. Choi, J. S. Brooks, D. L. Eaton, M. S. Al-Haik, M. Y. Hussaini, H. Garmestani, D. Li, K. Dahmen, *J. Appl. Phys.*, 2003, **94**, 6034.
7 R. Andrews, D. Jacques, A. M. Rao, T. Rantell, F. Derbyshire, Y. Chen, *Appl. Phys. Lett.*, 1999, **75**, 1329.
8 X. Ren, G. D. Seidel, *J. Intell. Mater. Syst. Struct.*, 2013, **24**, 1459.
9 S. Xu, O. Rezvanian, M. A. Zikry, *Smart Mater. Struct.*, 2013, **22**, 055032
10 K. Parmar, M. Mahmoodi, C. Park, S. S. Park, *Smart Mater. Struct.*, 2013, **22**, 075006.
11 R. Rahman, P. Servati, *Nanotechnology*, 2012, **23**, 055703.
12 N. Hu, Y. Karube, M. Arai, T. Watanabe, C. Yan, Y. Li, Y. L. Liu, H. Fukunaga, *Carbon*, 2010, **48**, 680.
13 T. C. Theodosiou, D. A. Saravanos. *Compos. Sci. Technol.*, 2010, **70**, 1312.
14 Z. F. Wang, X. Y. Ye, *Nanotechnology*, 2013, **24**, 265704.
15 T. W. Tombler, C. W. Zhou, L. Alexseyev, J. Kong, H. J. Dai, L. Liu, C. S. Jayanthi, M. J. Tang, S. Y. Wu, *Nature*, 2000, **405**, 769.
16 M. B. Nardelli, J. Bernholc, *Phys. Rev. B.*, 1999, **60**, R16338.
17 A. Rochefort, D. R. Salahub, P. Avouris, Chem. *Phys. Lett.*, 1998, **297**, 45.
18 E. D. Minot, Y. Yaish, V. Sazonova, J. Y. Park, M. Brink, P. L. McEuen, *Phys. Rev. Lett.*, 2003, **90**, 156401.
19 M. S. Fuhrer, J. Nygard, L. Shih, M. Forero, Y. G. Yoon, M. S. C. Mazzoni, H. J. Choi, J. Ihm, S. G. Louie, A. Zettl, *Science*, 2000, **288**, 494.
20 T. Hertel, R. E. Walkup, P. Avouris, *Phys. Rev. B.*, 1998, **58**, 13870.
21 R. S. Ruoff, J. Tersoff, D. C. Lorents, S. Subramoney, B. Chan, *Nature*, 1993, **364**, 514.
22 I. Palaci, S. Fedrigo, H. Brune, C. Klinke, M. Chen, E. Riedo, *Phys. Rev. Lett.*, 2005, **94**, 175502.
23 Y. H. Yang, W. Z. Li, *Appl. Phys. Lett.*, 2011, **98**, 041901.
24 C. Bower, R. Rosen, L. Jin, J. Han, O. Zhou, *Appl. Phys. Lett.*, 1999, **74**, 3317.
25 X. D. Yang, P. F. He, H. J. Gao, *Nano Res.*, 2011, **4**, 1191.
26 X. Peng, F. Tang, A. Copple, *J. Phys.: Condens. Matter.*, 2012, **24**, 075501.
27 W. S. Bao, S. A. Meguid, Z. H. Zhu, Y. Pan, G. J. Weng, *Mech. Mater.*, 2012, **46**, 129.
28 S. Gong, Z. H. Zhu, E. I. Haddad, *J. Appl. Phys.*, 2013, **114**, 074303.
29 S. Gong, Z. H. Zhu, *Polymer*, 2014, **55**, 4136.
30 S. Gong, Z. H. Zhu, S. A. Meguid, *Polymer*, 2014, **55**, 5488.
31 B. L. Wardle, D. S. Saito, E. J. Garcıa, A. J. Hart, R. G. Villoria, E. A. Verploegen, *Adv. Mater.*, 2008, **20**, 2707.
32 A. I. Oliva-Aviles, F. Aviles, V. Sosa, *Carbon*, 2011, **49**, 2989.
33 T. Kimura, H. Ago, M. Tobita, S. Ohshima, M. Kyotani, M. Yumura, *Adv. Mater.*, 2002, **14**, 1380.
34 N. Akima, Y. Iwasa, S. Brown, A. M. Barbour, J. Cao, J. L. Musfeldt, *Adv. Mater.*, 2006, **18**, 1166.
35 S. Liu, Y. Liu, H. Cebeci, R. G. de Villoria, J. H. Lin, B. L. Wardle, Q. M. Zhang, *Adv. Funct. Mater.*, 2010, **20**, 3266.
36 E. Camponeschi, R. Vance, M. Al-Haik, H. Garmestani, R. Tannenbaum, *Carbon*, 2007, **45**, 2037.
37 A. Maiti, A. Svizhenko, M. P. Anantram, *Phys. Rev. Lett.*, 2002, **88**, 126805.
38 H. J. Li, W. G. Lu, J. J. Li, X. D. Bai, C. Z. Gu, *Phys. Rev. Lett.*, 2005, **95**, 086601
39 N. Hu, Y. Karube, C. Yan, Z. Masuda, H. Fukunaga, *Acta Mater.*, 2008, **56**, 2929.
40 M. Taya, W. J. Kim, K. Ono, *Mech. Mater.*, 1997, **28**, 53.
41 B. Harris, *Engineering composite materials*, Institute of metals, London, **1986**.
42 L. A. Girifalco, M. Hodak, R. S. Lee, *Phys. Rev. B.*, 2000, **62**, 13104.
43 D. K. Davies, *J. Phys. D: Appl. Phys.*, 1969, **2**, 1533.
44 F. Du, J. E. Fischer, K. I. Winey, *Phys. Rev. B.*, 2005, **72**, 121404.
45 B. Hu, N. Hu, Y. Li, K. Akagi, W. Yuan, T. Watanabe, Y. Cai, *Nanoscale Res. Lett.*, 2012, **7**, 402.
46 G. Yin, N. Hu, Y. Karube, Y. L. Liu, Y. Li, H. Fukunaga, *J. Compos. Mater.*, 2011, **45**, 1315.
47 T. Kimura, H. Ago, M. Tobita, S. Ohshima, M. Kyotani, M. Yumura, *Adv. Mater.*, 2002, **14**, 1380.

